Supporting Information

Composite Salt in Porous Metal-Organic Frameworks for Adsorption Heat Transformation

Luis Garzón-Tovar[†], Javier Pérez-Carvajal[†], Inhar Imaz*[†] and Daniel Maspoch*[†‡]

† Catalan Institute of Nanoscience and Nanotechnology (ICN2), CSIC and The Barcelona Institute of Science and Technology, Campus UAB, Bellaterra, 08193 Barcelona, Spain.

‡ ICREA, Pg. Lluís Companys 23, 08010 Barcelona, Spain

E-mail: inhar.imaz@icn2.cat, daniel.maspoch@icn2.cat

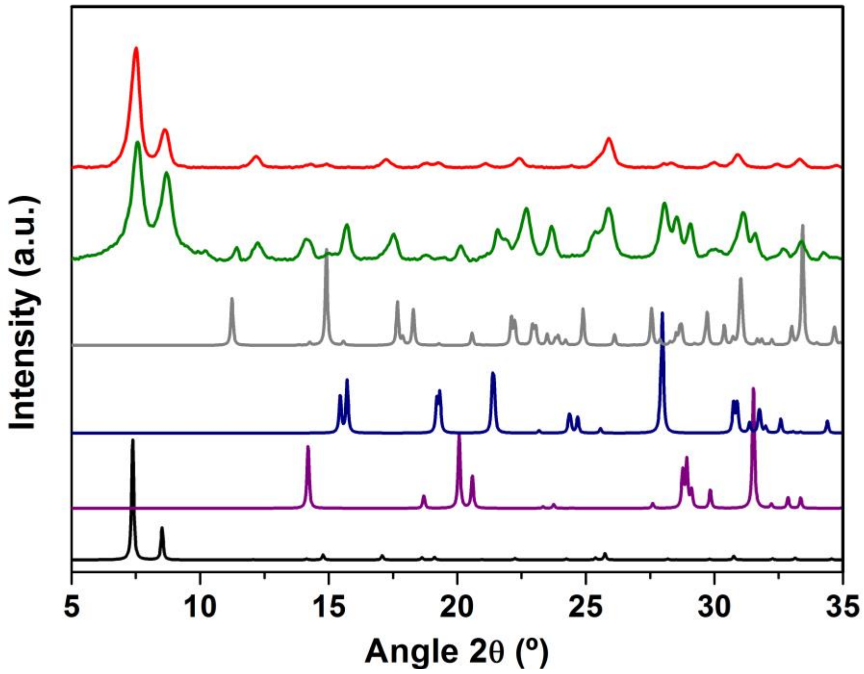

Figure S1. XRPD patterns of the $CaCl_2$@UiO-66_38 (green) and after $CaCl_2$ removal (red), compared to the simulated powder pattern for UiO-66 (black), $CaCl_2 \cdot 2H_2O$ (purple), $CaCl_2 \cdot 4H_2O\gamma$ (dark blue) and $CaCl_2 \cdot 4H_2O\beta$ (grey).

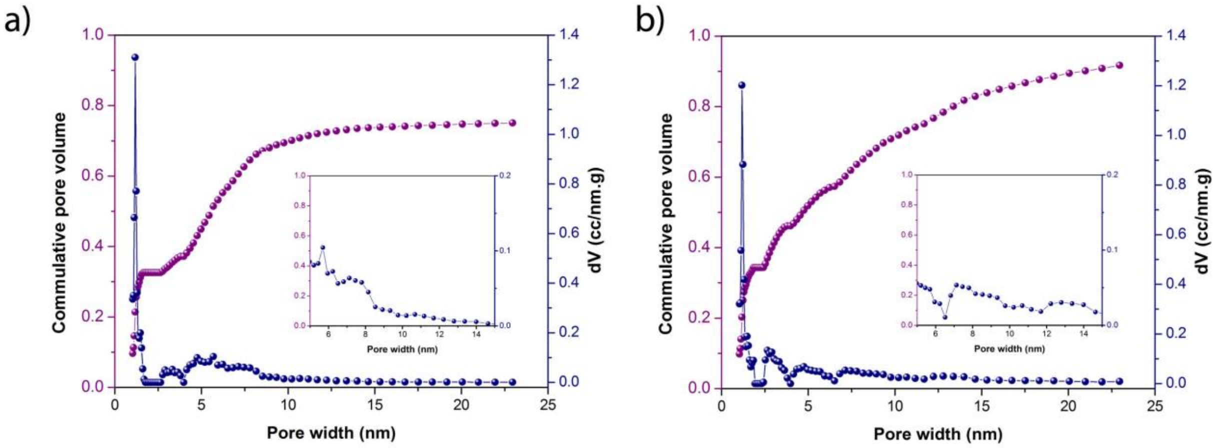

Figure S2. a) Pore size distribution of UiO-66 superstructures. b) Pore size distribution of $CaCl_2$@UiO-66_38 after $CaCl_2$ removal. The pore size distribution was calculated using NDFT slit pore equilibrium model for carbon at 77 K.

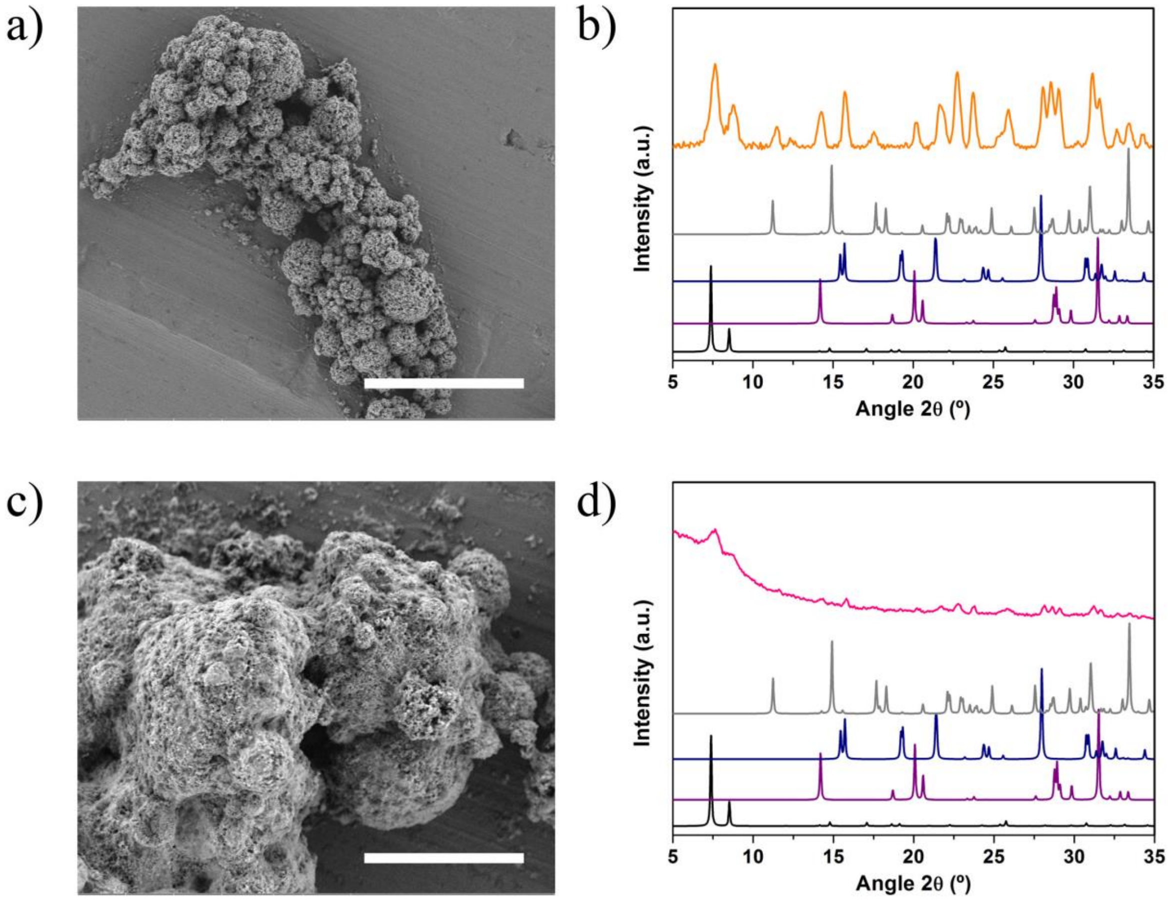

Figure S3. a) FESEM image of the $CaCl_2$@UiO-66_64. b) XRPD patterns of the $CaCl_2$@UiO-66_64 (orange) compared to the simulated powder pattern for UiO-66 (black), $CaCl_2{\cdot}2H_2O$ (purple) $CaCl_2{\cdot}4H_2O\gamma$ (dark blue) and $CaCl_2{\cdot}4H_2O\beta$ (grey). c) FESEM image of the composite prepared with a molar ratio of 1:6.4 (Zr^{4+} : $CaCl_2$). d) XRPD patterns of the composite (pink) compared to the simulated powder pattern for UiO-66 (black), $CaCl_2{\cdot}2H_2O$ (purple) and $CaCl_2{\cdot}4H_2O$ (dark blue). Scale bar: 20 µm (a) and 5 µm (c)

Table S1. Content of Ca in the composites estimated by digesting the as-made samples (previously outgassed at 200 ºC under vacuum) in H_2SO_4 at 50 ºC and analysed by ICP-OES.

Composite	Initial molar ratio Zr:Ca	Determined molar ratio Zr:Ca	% $CaCl_2$ (*w/w*)
$CaCl_2$@UiO-66	1:1.6	1:1.5	38
	1:2.6	1:2.5	50
	1:3.2	1:2.8	53
	1:4.8	1:4.4	64
$CaCl_2$@UiO-66-NH_2	1:1.6	1:1.5	38
Composite	**Initial molar ratio Zr:Li**	**Determined molar ratio Zr:Li**	**% LiCl (*w/w*)**
LiCl@UiO-66	1:1.6	1:1.6	19

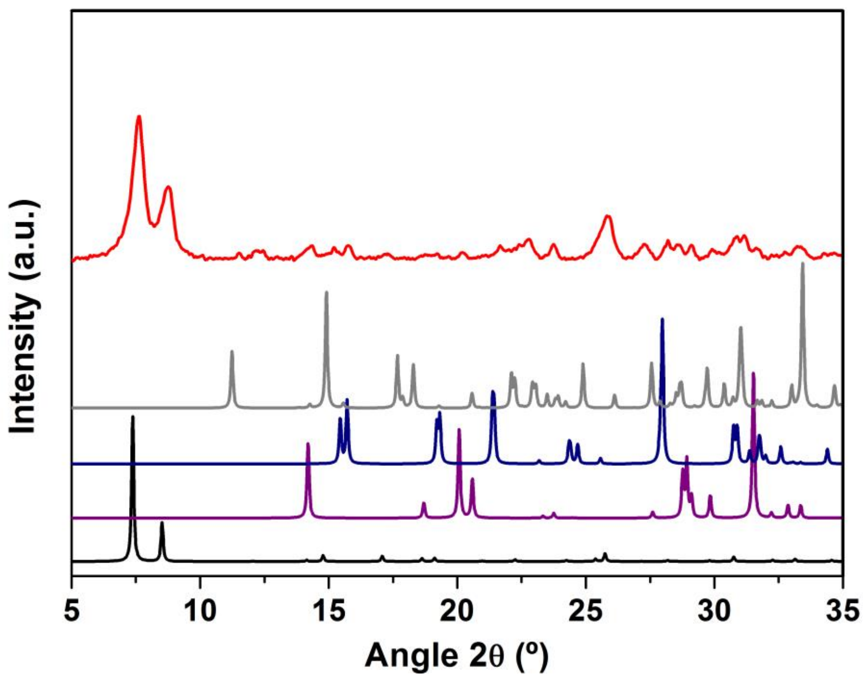

Figure S4. XRPD patterns of $CaCl_2$@UiO-66-NH_2_38 (red) compared to the simulated powder pattern for UiO-66 (black), $CaCl_2·2H_2O\gamma$ (purple), $CaCl_2·4H_2O$ (dark blue) and $CaCl_2·4H_2O\beta$ (grey).

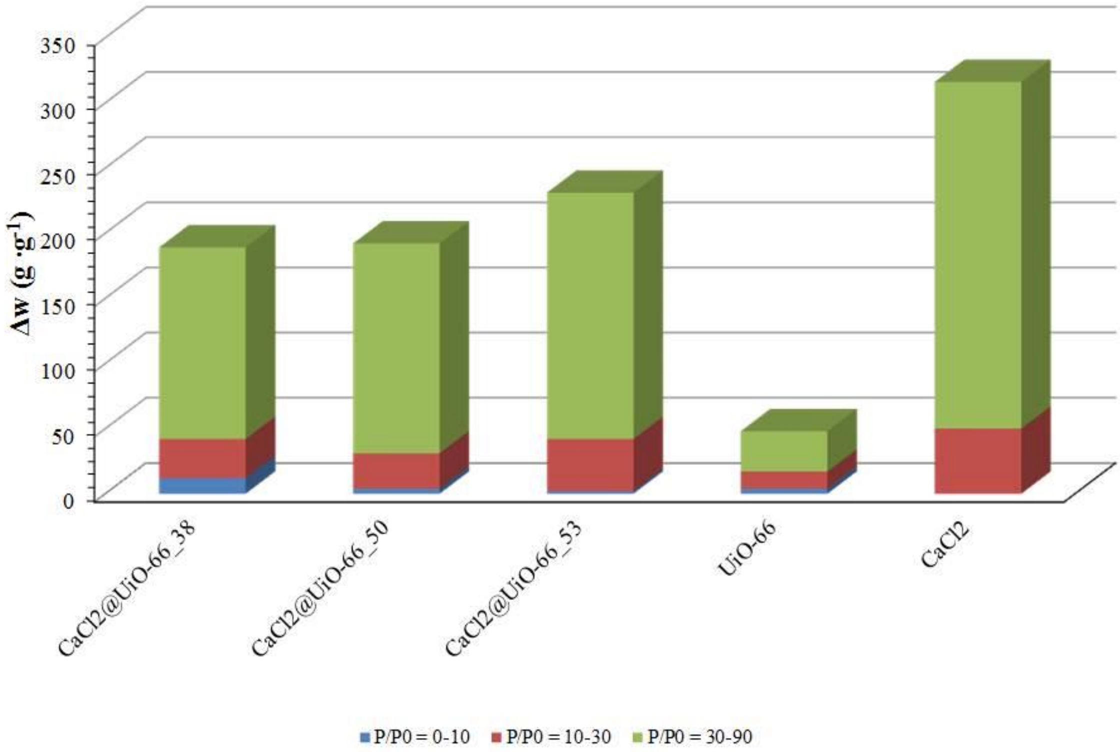

Figure S5. Working capacity calculated from the water isotherms for the composites, pristine UiO-66 and $CaCl_2$.

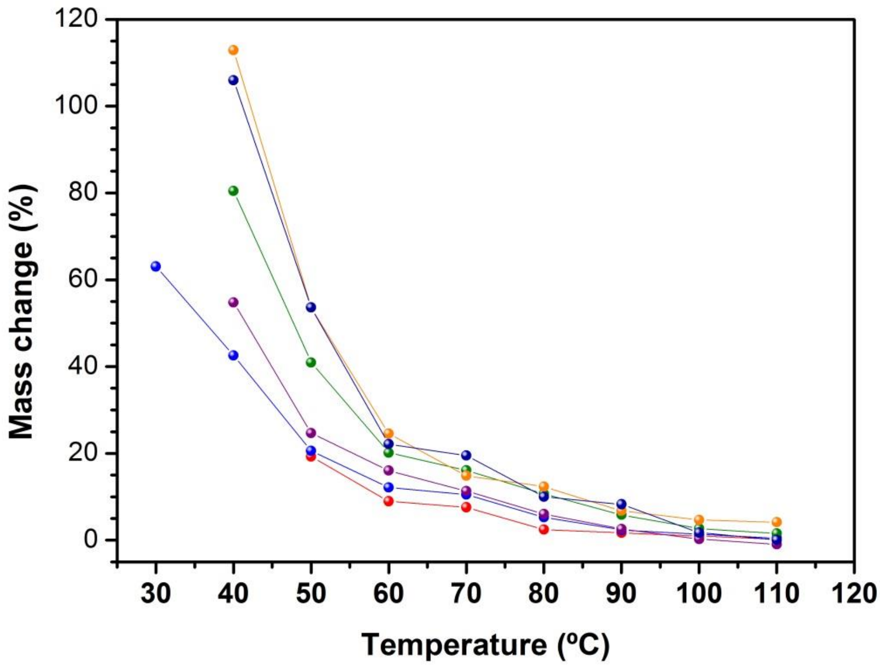

Figure S6. Water adsorption isobars of $CaCl_2$@UiO-66_53 at vapor pressures of 0.7 (red), 1.2 (blue), 2.4 (purple), 3.7 (green), 4.2 (dark blue) and 5.6 kPa (orange).

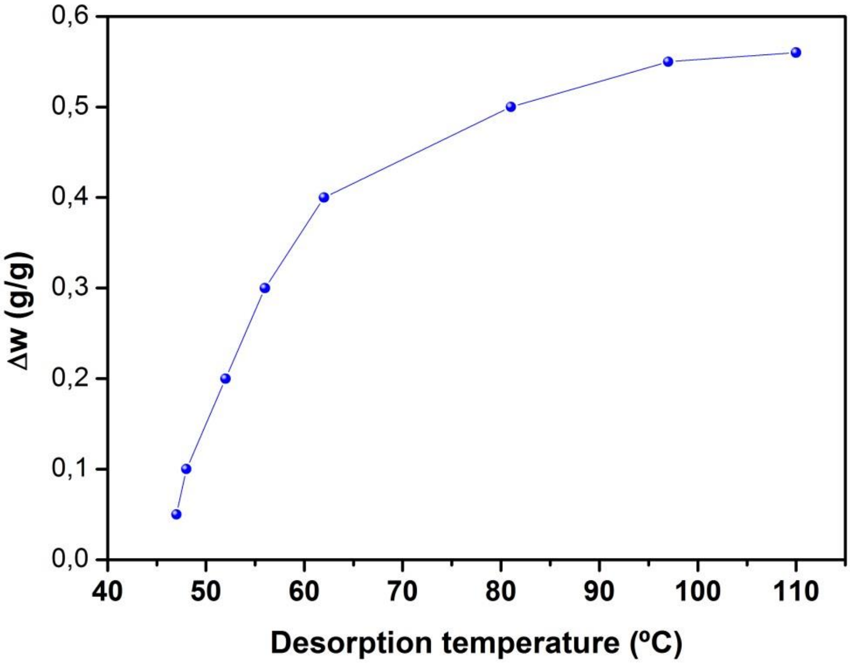

Figure S7. Working capacity as a function of the desorption temperature for the $CaCl_2$@UiO-66_53/water pair.

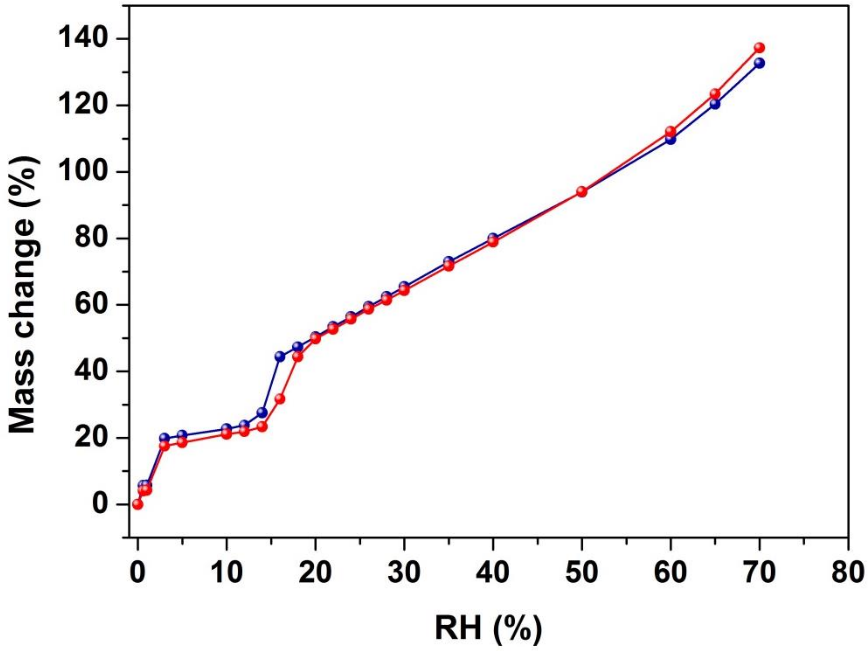

Figure S8. Water adsorption isotherms of $CaCl_2$@UiO-66_53 at 25 ºC (blue), 40 ºC (red).

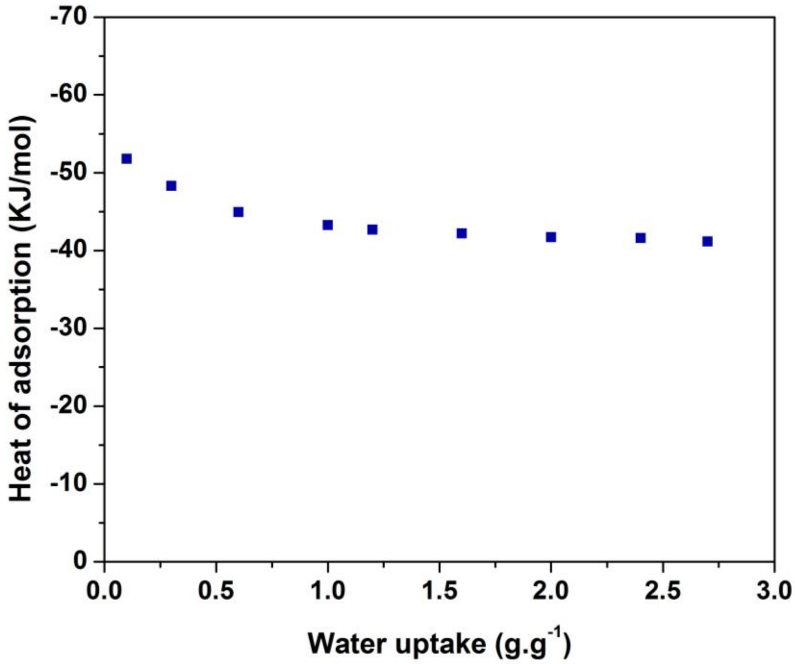

Figure S9. Heat of adsorption of $CaCl_2$@UiO-66_53.

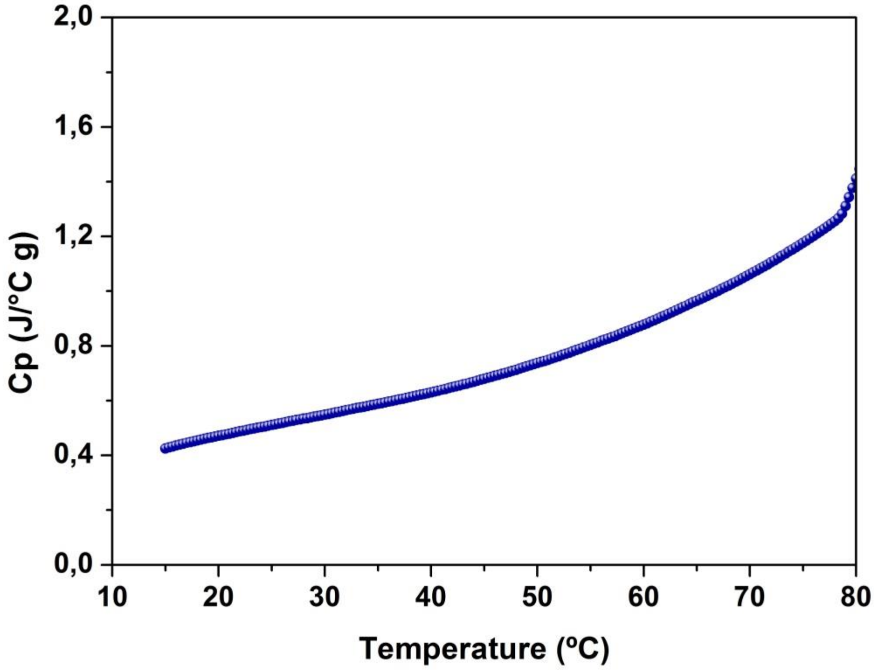

Figure S10. Heat capacity as a function of the desorption temperature for $CaCl_2$@UiO-66_53.